

Evaluation of diffuse and preferential flow pathways of infiltrated precipitation and irrigation using oxygen and hydrogen isotopes

Bin Ma¹ · Xing Liang^{2,1} · Shaohua Liu³ · Menggui Jin⁴ · John R. Nimmo⁵ · Jing Li¹

Received: 14 June 2016 / Accepted: 19 December 2016 / Published online: 7 January 2017
© Springer-Verlag Berlin Heidelberg 2017

Abstract Subsurface-water flow pathways in three different land-use areas (non-irrigated grassland, poplar forest, and irrigated arable land) in the central North China Plain were investigated using oxygen (^{18}O) and hydrogen (^2H) isotopes in samples of precipitation, soils, and groundwater. Soil water in the top 10 cm was significantly affected by both evaporation and infiltration. Water at 10–40 cm depth in the grassland and arable land, and 10–60 cm in poplar forest, showed a relatively short residence time, as a substantial proportion of antecedent soil water was mixed with a 92-mm storm infiltration event, whereas below those depths (down to 150 cm), depleted $\delta^{18}\text{O}$ spikes suggested that some storm water bypassed the shallow soil layers. Significant differences, in soil-water content and $\delta^{18}\text{O}$ values, within a small area, suggested that the proportion of immobile soil water and water flowing in subsurface pathways varies depending on local vegetation cover, soil characteristics and irrigation

applications. Soil-water $\delta^{18}\text{O}$ values revealed that preferential flow and diffuse flow coexist. Preferential flow was active within the root zone, independent of antecedent soil-water content, in both poplar forest and arable land, whereas diffuse flow was observed in grassland. The depleted $\delta^{18}\text{O}$ spikes at 20–50 cm depth in the arable land suggested the infiltration of irrigation water during the dry season. Temporal isotopic variations in precipitation were subdued in the shallow groundwater, suggesting more complete mixing of different input waters in the unsaturated zone before reaching the shallow groundwater.

Keywords Stable isotopes · Unsaturated zone · Diffuse flow · Preferential flow · China

Introduction

Soil water is the transition between precipitation and groundwater, and knowledge about subsurface soil-water flow pathways in the unsaturated zone is hence important for water resources management and for analyzing pollutant transfer to the aquifer (Jin et al. 1999; Liu et al. 2015; Nimmo 2005; Rusjan et al. 2008). Stable isotopes of oxygen (^{18}O) and hydrogen (^2H) are conservative and are, as molecules of water, naturally supplied by precipitation. Their proportions are altered only by physical processes like mixing with isotopically different waters or evaporation in the unsaturated zone, and thus can provide time-integrated information on subsurface hydrological processes in soil, including evaporation (Allison and Barnes 1983; Barnes and Allison 1988; Darling and Bath 1988; Hsieh et al. 1998; Liu et al. 1995), infiltration and downward percolation (Gazis and Feng 2004; Mathieu and Bariac 1996; McGuire et al. 2002; Mueller et al. 2014; Song et al. 2009; Stump and Maloszewski 2010), and

✉ Bin Ma
mabiniso@126.com

✉ Xing Liang
xliang@cug.edu.cn

¹ Present address: School of Environmental Studies, China University of Geosciences, Wuhan 430074, China

² Hubei Key Laboratory of Wetland Evolution & Ecological Restoration, School of Environmental Studies, China University of Geosciences, Wuhan 430074, China

³ Key Laboratory of Karst Dynamics, Institute of Karst Geology, Chinese Academy of Geological Sciences, Guilin 541004, China

⁴ State Key Laboratory of Biogeology and Environmental Geology, China University of Geosciences, Wuhan 430074, China

⁵ US Geological Survey, 345 Middlefield Road Mail Stop 420, Menlo Park, CA 94025, USA

residence time in subsurface water (Asano et al. 2002; DeWalle et al. 1997; Kabeya et al. 2007; Lee et al. 2007; McGuire et al. 2002; O'Driscoll et al. 2005; Rodgers et al. 2005). The rationale for using stable oxygen and hydrogen isotopic compositions in tracing subsurface water pathways is their seasonal as well as event-based or episodic variability in precipitation (Allen et al. 2015; DeWalle et al. 1997; Lee et al. 2007; O'Driscoll et al. 2005; Robertson and Gazis 2006).

The infiltration of precipitation is affected by a complex interplay of factors including the characteristics of precipitation (Stumpp and Maloszewski 2010; Wang et al. 2016), soil texture and structure (Huo et al. 2014; Li et al. 2015; Mathieu and Bariac 1996), topography (Dahlke et al. 2012; Hopp and McDonnell 2009; Lv et al. 2013; Mueller et al. 2014; Zhao et al. 2013), vegetation (Brodersen et al. 2000; Liu et al. 2015; Song et al. 2011; Stumpp et al. 2009a, b), and spatial and temporal scales (Hsieh et al. 1998; Li et al. 2015; Robertson and Gazis 2006; Stumpp and Hendry 2012). In general, there are two types of major soil-water movement: diffuse flow and preferential flow (Nimmo 2005). Diffuse flow is driven by gradients of soil-water potential, mixing with and forcing portions of the preexisting soil water to also flow. Preferential flow channels water through discrete pathways and bypasses portions of the medium (Nimmo 2005, 2012). A number of studies have emphasized the importance of preferential flow processes influenced by the fissures and macropores produced by cracks, plant roots, earthworm burrows, etc. (Hangen et al. 2005; Hardie et al. 2011; Mathieu and Bariac 1996; Nimmo 2005, 2010, 2012; Nimmo and Mitchell 2013; Stumpp and Maloszewski 2010).

Several factors are critical to determining the relative proportion of diffuse and preferential flow that occurs (Nimmo 2012). Antecedent soil moisture strongly influences the type, depth and rate of water movement (Dahlke et al. 2012; Hardie et al. 2011; Jaynes et al. 2001; Kung et al. 2000; Nimmo 2005; Zhao et al. 2013). Hardie et al. (2011) found that increased preferential flow correlated with decreased antecedent soil moisture, in contrast to studies such as Jaynes et al. (2001) and Kung et al. (2000). Zhao et al. (2013) concluded that high antecedent soil moisture and high rain intensity favor the generation of diffuse flow. Stumpp and Maloszewski (2010) quantified preferential flow in the unsaturated zone of cropped soils using a lumped dispersion model based on the hydrological and stable isotope data and concluded that high-intensity rain events could contribute to much preferential flow even if the soil is initially dry. Liu et al. (2015) found that rainwater from a small precipitation event penetrated soil to considerable depth, which suggests a dominance of preferential flow with little precipitation when the water content was low. These studies indicate that soil-water movement depends strongly on rain intensity and antecedent soil moisture.

Comparison of stable isotopic compositions is a powerful tool for investigating the mechanisms of soil-water movement

(Gazis and Feng 2004; Li et al. 2007; Liu et al. 2015; O'Driscoll et al. 2005; Song et al. 2009, 2011; Zhao et al. 2013). Rainstorms that differ in isotopic composition may cause variations in soil-water isotopic profiles. Diffuse flow may result in an abrupt isotopic front that delineates isotope ratios representing antecedent pore water from recent infiltration within the soil profile, whereas preferential flow frequently results in isotopic composition spikes deeper in the soil profile (Gazis and Feng 2004; Mathieu and Bariac 1996; O'Driscoll et al. 2005).

In the semi-arid North China Plain (NCP), precipitation varies seasonally. Storms during the rainy season (June to September) account for 70% of the annual precipitation (Song et al. 2009, 2011; Wang et al. 2008). During the dry season (October to May), farmers irrigate to supply crop water needs (Lin et al. 2013; Ma et al. 2016). By measuring the stable isotopic compositions of precipitation, soil water and groundwater, Li et al. (2007) and Song et al. (2009, 2011) investigated rainy-season preferential flow processes and groundwater recharge in the piedmont alluvial plain. Many other studies employing environmental tracers (chloride, fluoride and sulfate), artificial tracers (bromine; Lin et al. 2013; Wang et al. 2008), and thermonuclear tritium profiling (Jin et al. 2000; Rohden et al. 2010) also elucidate NCP recharge processes based on the assumption of diffuse flow. The infiltration and flow mechanisms, however, remain controversial.

The objective of this study is to improve the understanding of subsurface water flow pathways by investigating the transformation of the meteoric isotopic signal through the upper unsaturated zone for sites with different vegetated soils in the central alluvial and lacustrine plain of NCP. In order to achieve this objective, the temporal variation of stable isotopic compositions in precipitation on a daily basis and in groundwater at biweekly intervals was monitored from April 2012 to October 2013. The soil profiles were simultaneously drilled and soil water was extracted for stable isotopic composition analysis both in the rainy and dry seasons.

Materials and methods

Site description

The North China Plain (Fig. 1a,b), located at 112°30'E–119°30'E and 34°46'N–40°25'N, with a population of more than 200 million and area of approximately 150,000 km², is an important region of China politically, economically, and agriculturally. The NCP consists of the piedmont plain, alluvial and lacustrine plain, and littoral plain, from west to east. It is bordered by the Taihang Mountains to the west and Bohai Sea to the east, by the Yanshan Mountains to the north, and the Yellow River to the south (Chen et al. 2003), where Quaternary aquifer systems developed at different depths

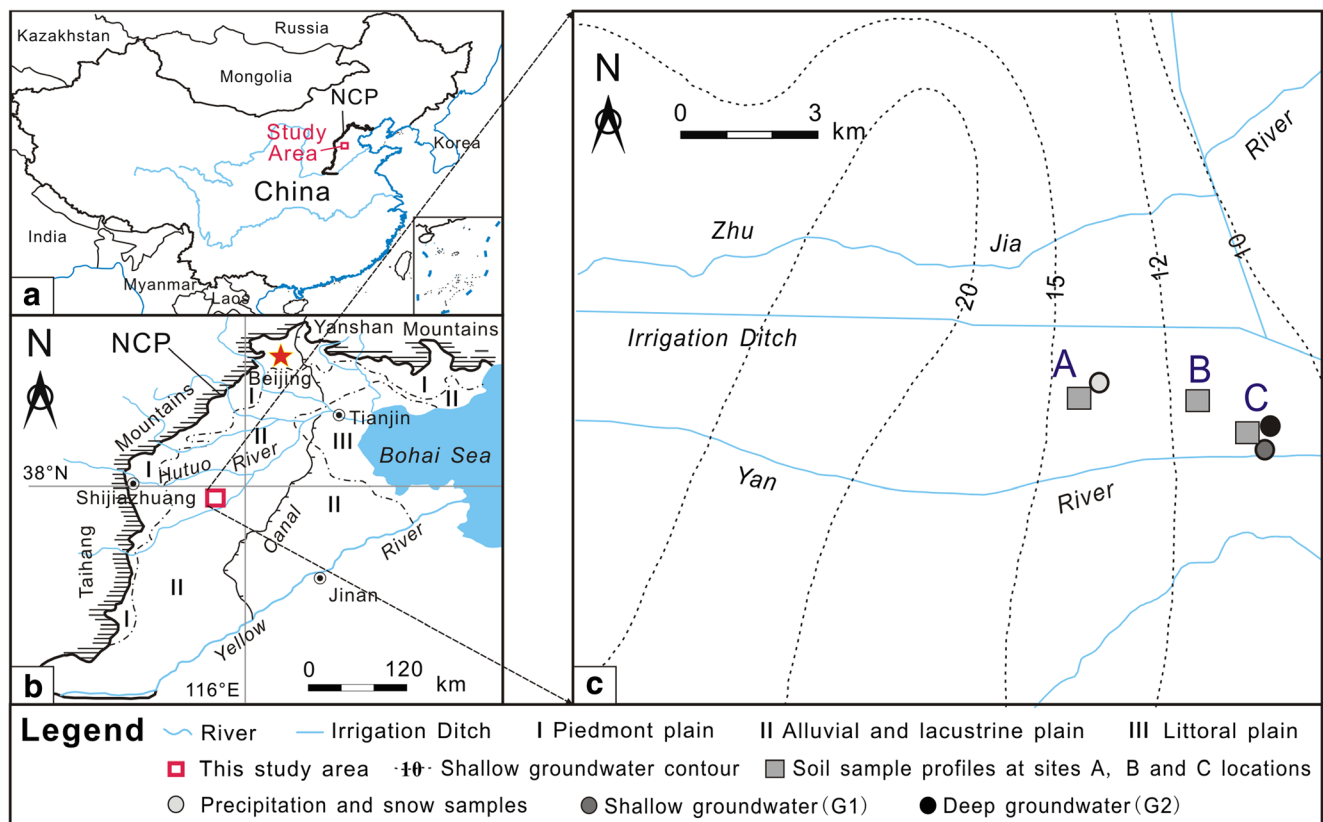


Fig. 1 The location of study area: **a** North China Plain (from Lin et al. 2013); **b** study area (from Chen et al. 2003); **c** sampling locations: soil sample profiles at sites A, B and C; the precipitation and snow samples

were collected at site A, the shallow groundwater (G1, deep < 50 m) and deep groundwater (G2, deep 230 m) were collected at site C

(Foster et al. 2004; Zhang et al. 1997). The thickness of Quaternary sediments varies considerably from 150 to 600 m. Fluvial deposits dominate in the piedmont plain, alluvial and lacustrine deposits in the central plain, and alluvial deposits with interbedded marine deposits in the littoral plain. The NCP has a middle-latitude continental semi-arid monsoon climate, with a mean annual temperature of 12–13 °C, and mean annual precipitation and potential evaporation of 500–600 mm and of 1,100–1,800 mm, respectively. Because of monsoonal influence, the rainy season (June to September) accounts for the abundant annual precipitation (70%) compared to the long dry season (October to May).

Groundwater is the main source of water supply of the NCP (Foster et al. 2004; Shi et al. 2014; Sun et al. 2015). Nearly 70% of the total water consumption is for agriculture (Ma et al. 2016). The long-term increased groundwater pumping has resulted in increasing thickness of unsaturated zone (Sun et al. 2015) and delay in the process of vertical recharge to the water table (Huo et al. 2014).

Cultivars of winter wheat and summer maize have frequently changed over time. In the arable land, winter wheat is usually planted in early October, and harvested during the first 10 days of June. Summer maize is planted immediately after wheat harvest and harvested at the end of September

(Sun et al. 2015). Flooding irrigation is conducted mainly during April to May and in October, of which approximate 70% is for wheat irrigation (Ma et al. 2016).

Field studies were conducted at three vegetated soils in the central alluvial and lacustrine plain of NCP (Fig. 1c). Site A and site B are non-irrigation land covered by grass (*Carex humili* and *C. lanceolata*) and poplar (*Ponulus hopeiensis*) respectively, while site C is managed as long-term arable land and used for irrigated winter wheat (*Triticum aestivum*) and summer maize (*Zea mays*). The land cover proportion by poplar, arable land and grass are roughly 0.18, 94.7 and 0.2%, respectively (Yang et al. 2007). The precipitation and snow samples were collected about 50 m away from the soil profiles at site A (Fig. 1c). The soil textures were defined according to the United States Department of Agriculture (USDA) soil texture classification (Gee and Or 2002). Soil profiles included sandy loam, silt loam, and loam and contained various proportions of sand, silt and clay (Fig. 2).

Sample collection

Water samples from precipitation, snowmelt, groundwater and soil water were collected for oxygen and hydrogen isotopic analyses from April 2012 to October 2013. Precipitation was

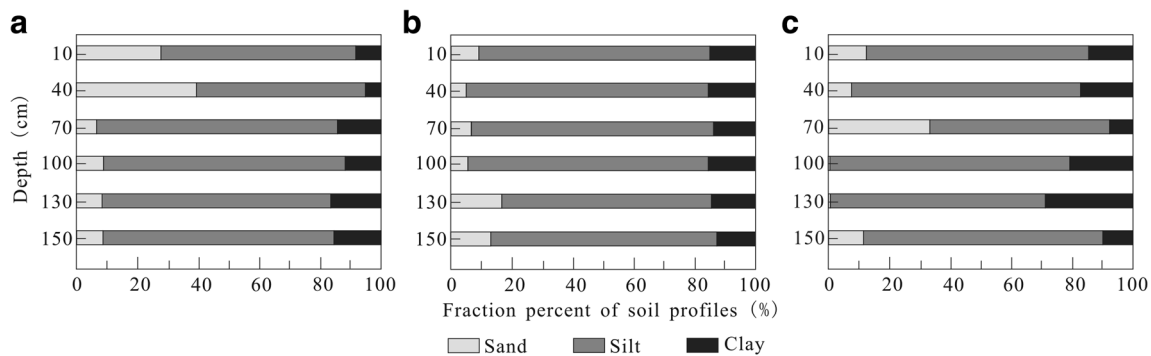


Fig. 2 The fraction percent of the soil grain size at the three sampling sites: **a** grassland at site A; **b** poplar forest at site B; **c** arable land (summer maize and winter wheat) at site C

collected at site A (ground surface elevation 17 m above sea level) in an all-weather rain gauge into which mineral oil was poured to minimize evaporation (Fig. 1c). Snow was sampled by collection at the ground surface in a polyethylene tray (O'Driscoll et al. 2005; diameter 50 cm) and retrieved manually in 500-ml plastic air-tight rain collectors to melt at room temperature. Samples were gathered as soon as possible after a precipitation or snow event. The oxygen isotopic composition of throughfall and open rainfall is different for individual storm events (DeWalle and Swistock 1994), and from hereafter precipitation, snowmelt and throughfall is referred to as precipitation.

Deep groundwater (G2, well depth 230 m, for irrigating) and shallow groundwater (G1, well depth < 50 m with groundwater depth 9.0 m) were collected at approximately biweekly intervals during the period of August 2012–October 2013 at site C (Fig. 1c). The deep groundwater was collected from the G2 well pumping station. In order to avoid contamination or evaporation, the well was pumped for a minimum of 5 min before sampling, and the water samples were taken directly at the outlet of the pump. Shallow groundwater was collected from the water level surface at the G1 well, about 100 m south of the G2 well collector. The water table depth of G1 well is as deep as 9.0 m; the fractionation of the surface well water is negligible when sampling.

For soil-water isotope values, soil samples were taken from a plot smaller than 5×2 m at each site, covered by different vegetation, on 24 July, 2, 4 and 13 August 2012 during the rainy season, and 22 October 2012 and 18 April 2013 during the dry season. At sites A, B, and C, soil samples were collected with a manual auger from every 10-cm interval between 10 and 150 cm depth (main root zone of 0–120 cm in the arable land). The samples were placed in glass bottles and sealed with wax and packaging tape immediately after sampling to prevent fractionation caused by evaporation. All soil samples were stored in a deep freezer and kept at -18 °C until analysis, which occurred within 150 days from the sample collection (Robertson and Gazis 2006; Sugimoto et al. 2003). Soil-water content (percent by volume) was measured

manually at the depth of soil sampling with time domain reflectometry (TDR, MPM-160, Australia, ICT International Pty Ltd.).

Isotope analysis

Cryogenic vacuum extraction is a widely utilized method for water extractions from unsaturated soil samples (Araguás-Araguás et al. 1995; Koeniger et al. 2011; Orłowski et al. 2013, 2016; Shurbaji and Phillips 1995), which has been shown to yield as accurate and reproducible results as other extraction methods (Ignatov et al. 2013; Ingraham and Shadel 1992; Revesz and Woods 1990; Walker et al. 1994). Past and more recent studies (Araguás-Araguás et al. 1995; Koeniger et al. 2011; Orłowski et al. 2013, 2016; Walker et al. 1994; West et al. 2006) have shown that cryogenic extraction conditions (extraction time, temperature, vacuum threshold) and physicochemical soil properties can impact the extracted soil-water isotope results.

In this study, two extraction systems were applied, using just one independent extraction line and a single distillation system. The extraction pressures were as low as <1.0 Pa. The extraction temperature ranged from 75 to 100 °C. The extraction time varied from 4 to 7 h. The details on the laboratory procedure are similar to Shurbaji et al. (1995).

In order to validate the accuracy and reproducibility of the $\delta^{18}\text{O}$ and $\delta^2\text{H}$ values by this cryogenic vacuum extraction, two sets of extra experiments employing five liquid water samples and five silt loam soil samples were set up. The first set of experiments was performed with liquid water of known isotopic composition to test the accuracy of this vacuum distillation method. The liquid water samples were taken during a rainstorm on 28 June 2012 at Wuhan, China ($\delta^{18}\text{O}$ and $\delta^2\text{H}$ values of -3.92 and -14.6‰). Around 100-ml of liquid water was split into five individual water samples, which were distilled for 4 h (at extraction temperature 75 °C). The second set of experiments was aimed at evaluating the reproducibility and accuracy of the $\delta^{18}\text{O}$ and $\delta^2\text{H}$ values distilled from soil. The silt loam was sampled from site B in the study area

(Fig. 1c). In the first step, the silt loam soil sample was oven dried for 24 h at 120 °C. Around 5 kg of oven-dried silt loam was split into five individual samples and evenly hydrated with 20 ml of water of known isotopic composition (liquid water in the first experiments). Extraction was done for 7 h at 100 °C. The results are given in Table 1.

After the split-sample experiments, approximately 150 g soil, for all samples collected from the study area, was subjected to continuous heating for 7 h, with final extraction temperature approaching 100 °C. Approximately 10–40 ml of extracted water was trapped at liquid nitrogen temperature. The details on the laboratory procedure are similar to Shurbaji et al. (1995). The soil remaining after vacuum distillation was removed and dried in the oven at 120 °C for 24 h, demonstrating that the complete extraction from the original soil water was more than 99.90% (in terms of the weight) after the vacuum distillation, based on 81 soil samples. Consequently, all of the interstitial soil water, which was a combination of tightly bound and relatively mobile water (Araguás-Araguás et al. 1995; Landon et al. 1999), was extracted at 100 °C extraction temperature; therefore, the sample size and heating time and temperature were feasible for complete extraction even though fractionation occurred during the boiling process.

The measurements for oxygen and hydrogen isotope ratios were conducted at the State Key Laboratory of Biogeology and Environmental Geology, China University of Geosciences, Wuhan, China. All stable isotopic compositions were measured using a Finnigan MAT-253 mass spectrometer (Thermo Fisher, USA, manufactured in Bremen, Germany), with the TC/EA method (Gong et al. 2007). Results were presented in ‰ with respect to the Vienna Standard Mean Ocean Water (VSMOW, Gonfiatini 1978) according to

$$\delta_{\text{sample}}(\text{‰}) = \left(R_{\text{sample}} / R_{\text{standard}} - 1 \right) \times 1000 \quad (1)$$

where δ_{sample} is the isotope ratio of sample relative to the VSMOW, R is the $^2\text{H}/^1\text{H}$ or $^{18}\text{O}/^{16}\text{O}$ atomic ratio. The stable

isotopes ^2H and ^{18}O were measured with an analytical precision of 0.5‰ vs. VSMOW for $\delta^2\text{H}$ and of 0.1‰ for $\delta^{18}\text{O}$.

Results

Accuracy and reproducibility of the cryogenic vacuum extraction

The standard deviations (Table 1) for liquid water samples were 0.09‰ for $\delta^{18}\text{O}$ and 0.8‰ for $\delta^2\text{H}$, for silt loam soil-water samples were 0.15‰ for $\delta^{18}\text{O}$ and 0.77‰ for $\delta^2\text{H}$, respectively. Two soil-water samples showed slightly more depleted $\delta^{18}\text{O}$ values (−4.12 and −4.22‰; Table 1) than the initial hydrated water (−3.92‰). This was probably due to fractionation during distillation. In this study area, the soil types are sandy loam, silt loam, and loam (Fig. 2), and the fraction of clayey soil is overall less than 20% (at the depth of 130 cm at site C is 28.5%). The results (Table 1) showed that the proposed cryogenic vacuum extraction can achieve high accuracy for both liquid water samples and silt loam soil samples with low water content (around 2.0% by weight).

$\delta^{18}\text{O}$ and $\delta^2\text{H}$ values in precipitation and groundwater

The $\delta^{18}\text{O}$ and $\delta^2\text{H}$ values of daily precipitation samples and biweekly groundwater samples collected in the study area between April 2012 and October 2013 are presented in Figs. 3 and 4. The monitored local precipitation amount and temperature are shown in Fig. 5. Overall, the precipitation $\delta^{18}\text{O}$ and $\delta^2\text{H}$ values ranged from −12.0 to −1.7‰ and −98.9 to −13.3‰, respectively. The amount-weighted mean $\delta^{18}\text{O}$ and $\delta^2\text{H}$ values of precipitation in the dry season (−10.6 and −84.3‰, respectively) were more depleted than those in the rainy season (−7.6 and −63.2‰, respectively), with amount-weighted annual mean values of −7.9 and −65.7‰,

Table 1 Results of the extraction experiments with liquid water samples and silt loam soil samples doped with water of known isotopic composition

Sample no.	Vacuum distillation from liquid water			Vacuum distillation from soil		
	$\delta^{18}\text{O}$ (‰)	$\delta^2\text{H}$ (‰)	Sample size (ml)	$\delta^{18}\text{O}$ (‰)	$\delta^2\text{H}$ (‰)	Gravimetric water content (%)
WHP01	−4.05 ± 0.07	−15.4 ± 1	20	−4.12 ± 0.09	−13.9 ± 0.7	2.04
WHP02	−4.06 ± 0.03	−15.7 ± 0.7	20	−3.91 ± 0.09	−14.8 ± 0.1	1.93
WHP03	−3.94 ± 0.01	−14.2 ± 0.3	20	−3.86 ± 0.07	−15.2 ± 0.3	2.03
WHP04	−3.87 ± 0.07	−13.8 ± 0.3	20	−3.93 ± 0.03	−13.3 ± 0.5	2.11
WHP05	−3.90 ± 0.05	−14.5 ± 0	20	−4.22 ± 0.04	−14.7 ± 0.2	1.92
Average	−3.96	−14.72	-	−4.01	−14.38	-
SD	0.09	0.8	-	0.15	0.77	-

The $\delta^{18}\text{O}$ and $\delta^2\text{H}$ values for the liquid water sample and doping water were −3.92 and −14.6‰, respectively
SD standard deviation

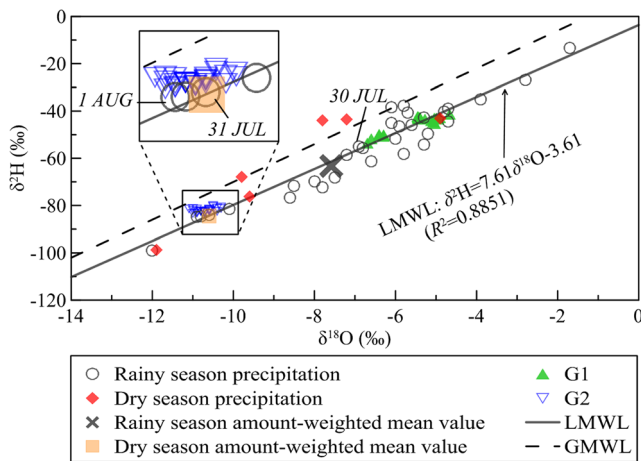


Fig. 3 Relationship between $\delta^{18}\text{O}$ and $\delta^2\text{H}$ values of precipitation at site A and shallow groundwater (G1, deep < 50 m) and deep groundwater (G2, deep 230 m) at site C during the period of April 2012–October 2013. 6.5, 76.9 and 8.7 mm precipitation happened on 30 July, 31 July and 1 August 2012 are indicated. *Dash line and solid line* correspond to the global meteoric water line (GMWL) and local meteoric water line (LMWL), respectively

respectively. The local meteoric water line (LMWL) can be defined by regression based on 37 precipitation $\delta^{18}\text{O}$ and $\delta^2\text{H}$ values (Fig. 3). Both the linear slope (7.6) and intercept (−3.7) of the LMWL are lower than that of the global meteoric water line (GMWL, 8 and 10, respectively; Craig 1961).

The $\delta^{18}\text{O}$ and $\delta^2\text{H}$ values in groundwater show much narrower range than those in precipitation, ranging from

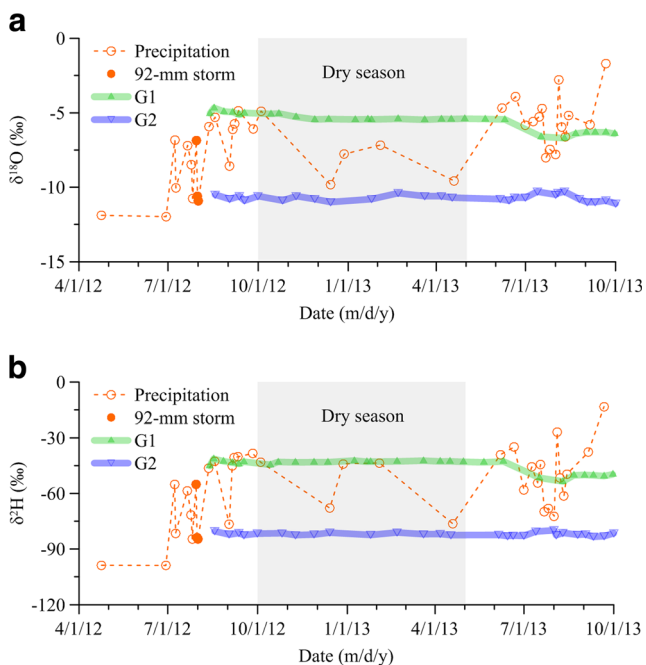


Fig. 4 Temporal variation of **a** $\delta^{18}\text{O}$ and **b** $\delta^2\text{H}$ values, in precipitation, shallow groundwater (G1, deep < 50 m) and deep groundwater (G2, deep 230 m) from April 2012 to October 2013. The orange solid circles indicate the 92-mm storm that occurred from 30 July to 1 August with the mean $\delta^{18}\text{O}$ and $\delta^2\text{H}$ values of −10.4 and −81.9‰

−6.7 to −4.7‰ and −53.5 to −41.3‰ with mean values of −5.5 and −45.1‰ for shallow groundwater (G1), and ranging from −11.1 to −10.3‰ and −83.4 to −79.9‰ with mean values of −10.7 and −82.1‰ for deep groundwater (G2), respectively. It is shown in Fig. 3 that the shallow groundwater samples fall along the upper part of the LMWL, while the deep groundwater samples plot in a tight cluster on the lower end of the LMWL (Fig. 3); whereas it is shown in Fig. 4 that the temporal variations of $\delta^{18}\text{O}$ and $\delta^2\text{H}$ values for both the shallow and deep groundwater are significantly smaller than those in precipitation.

Soil-water content and soil-water $\delta^{18}\text{O}$ values

The temporal variation of soil-water content (percent by volume) during the rainy season of 2012 is shown in Fig. 6. Soil-water content at sites A and C were higher than those at site B; the largest temporal variability was observed at site A, while at site C soil-water content was relatively steady from 24 July to 17 August 2012.

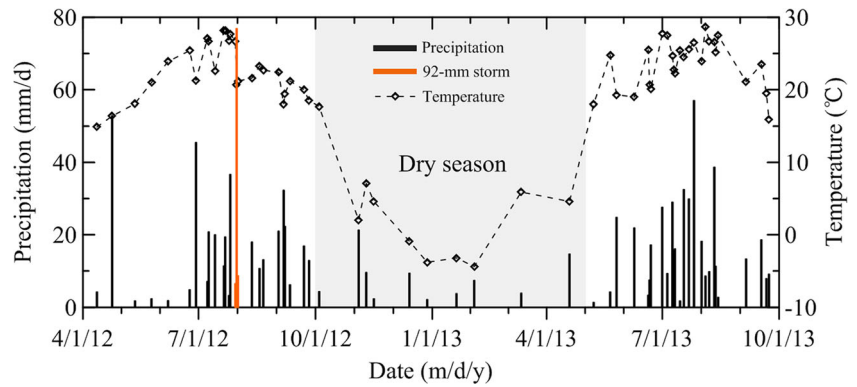
Figure 7 presents the vertical profiles of soil-water $\delta^{18}\text{O}$ values and soil-water content during the rainy season monitored on 24 July, and on 2, 4, and 13 August 2012. These dates fall before and after a large, continuous rainstorm event during 30 July to 1 August 2012 (total precipitation amount 92.1 mm, amount-weighted mean $\delta^{18}\text{O}$ −10.4‰, referred to hereafter as the “92-mm storm”). Soil-water $\delta^{18}\text{O}$ values were characterized by smaller variance for the three sites on 24 July before the 92-mm storm (site A from −9.4 to −6.0‰, site B from −7.0 to −4.1‰, and site C from −7.5 to −6.1‰, respectively) than those after the 92-mm storm on 2, 4, and 13 August (site A from −9.6 to −6.2‰, site B from −9.3 to −4.9‰, and site C from −9.6 to −6.4‰, respectively). Furthermore, the greatest variability of soil-water $\delta^{18}\text{O}$ values was observed at shallow depth rather than in the deeper depth (Fig. 7). Vertical profiles of soil-water $\delta^{18}\text{O}$ and soil-water content during the dry season collected on 22 October 2012 and 18 April 2013 are shown in Fig. 8. The soil profiles on 22 October 2012 and 18 April 2013 at site C were obtained 10 and 2 days later after irrigation, respectively, while there were no irrigation at sites A and B. The greatest variability was observed at site C affected by irrigation and the lowest variability was observed at site B (Fig. 8).

Discussion

Origin of groundwater based on $\delta^{18}\text{O}$ and $\delta^2\text{H}$ values

The $\delta^2\text{H}$ – $\delta^{18}\text{O}$ values (Fig. 3) for shallow groundwater (G1) and deep groundwater (G2) cluster at two distinct zones along the LMWL, indicating that both are local precipitation origins. Moreover, distinct isotopic compositions suggest two types of

Fig. 5 Daily precipitation amount and temperature at site A from April 2012 to October 2013. The snow depths were measured on a daily basis and converted from melted-snow depths to precipitation amount (15 mm snow approximately 1 mm snowmelt). The orange bars indicate the 92-mm storm occurred from 30 July to 1 August with the total amount 92.1 mm



origins for shallow and deep groundwater in the study area. Shallow groundwater samples cluster along the LMWL and were close to the precipitation during the rainy season (Fig. 3),

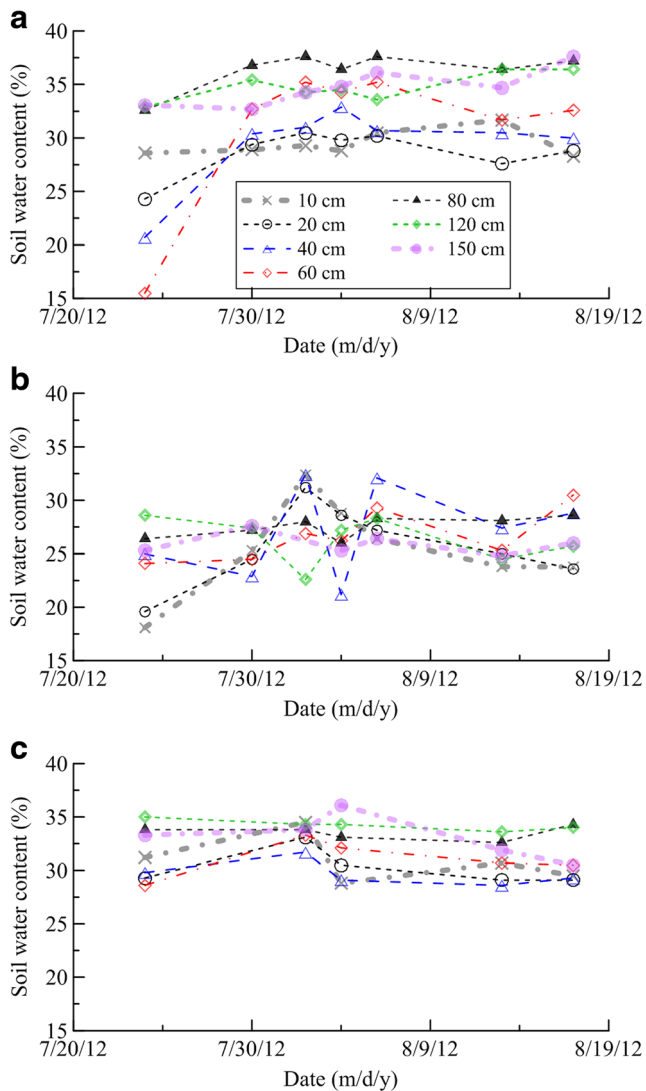


Fig. 6 Soil-water content (percent by volume) observed manually by TDR at 10, 20, 40, 60, 80, 120 and 150 cm at the three sites from July to August 2012. Sites a A, b B and c C

which might indicate that the isotopic composition of recharge was dominated by water from rainy season infiltration. The more enriched isotope values in shallow groundwater compared with the amount-weighted mean value of precipitation in the rainy season might indicate fractionation by evaporation during the soil-water infiltration. Two different origins might explain the isotopically depleted deep groundwater. One possibility is the meteoric origin during a period of colder climate than in modern times, and another possible origin is the lateral flow of snowmelt-derived groundwater from the adjacent mountain areas. These two possible origins of the deep groundwater were proved by previous studies in the NCP (Chen et al. 2003; Liu et al. 2010; Zhang 2005). Liu et al. (2010) indicated that altitude is the main geographic factor controlling the isotopic composition of precipitation in the NCP and the $\delta^{18}\text{O}$ value depletes 0.2‰ with elevation increasing 100 m; therefore, the recharge elevation of the deep groundwater could be estimated to be approximately 1,400 m by comparing the mean $\delta^{18}\text{O}$ value of deep groundwater (−10.7‰) at site C (elevation 18 m) with the value of local precipitation (mean $\delta^{18}\text{O}$ −7.9‰). Consequently, the data indicate that the source of groundwater withdrawn as irrigation in the study area is isotopically different from the local precipitation.

Isotopic temporal variations in precipitation and groundwater

Large temporal variations in isotopic compositions of precipitation from day to day are common. The precipitation showed substantial variation in the daily $\delta^{18}\text{O}$ and $\delta^2\text{H}$ values for both the dry season (−11.9 to −4.9‰ and −98.8 to −43.1‰, respectively) and rainy season (−12.0 to −1.7‰ and −98.9 to −13.3‰, respectively; Fig. 4). This highlighted the episodic $\delta^{18}\text{O}$ and $\delta^2\text{H}$ variability of precipitation, and thus permitted identification of the discrepant precipitation input in the unsaturated zone. Some depleted $\delta^{18}\text{O}$ and $\delta^2\text{H}$ values occurred in the rainy season of 2012 (29 June of −12.0 and −98.9‰; 9 July of −10.1 and −81.5‰; 26 July of −10.8 and −84.6‰; and 31 July of −10.6 and −83.9‰); these, however, resulted in a

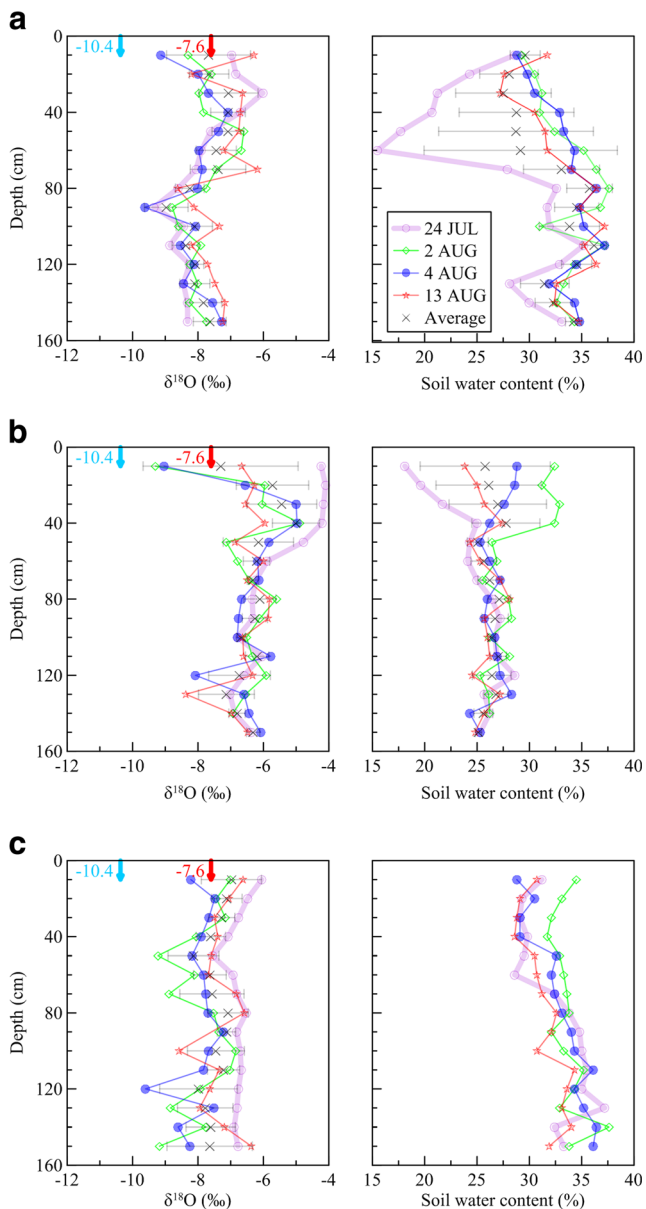


Fig. 7 Vertical profiles of soil-water $\delta^{18}\text{O}$ values and soil-water content (percent by volume) observed in the rainy season of 2012 at the three sites: **a** A, **b** B and **c** C. The accuracy of the cryogenic vacuum extraction for soil-water $\delta^{18}\text{O}$ and $\delta^2\text{H}$ are 0.15 and 0.77‰, respectively. The sky blue arrows indicate the 92-mm storm that occurred from 30 July to 1 August with the amount-weighted mean $\delta^{18}\text{O}$ value of -10.4‰ . The red arrows indicate the precipitation during the rainy season with amount-weighted mean $\delta^{18}\text{O}$ value of -7.6‰

less well-defined seasonal cycle of precipitation stable isotopic compositions (Fig. 4).

Highly variable $\delta^{18}\text{O}$ and $\delta^2\text{H}$ values from the 92-mm storm were observed on the basis of sequential daily samples collection (30 July of -6.9 and -55.0‰ , amount 6.5 mm; 31 July of -10.6 and -83.9‰ , amount 76.9 mm; 1 August of -10.9 and -84.7‰ , amount 8.7 mm; seen in Figs. 3, 4, and 5). In a study of meteoric water along a climate gradient on the east side of the Cascade Mountains (Washington, USA),

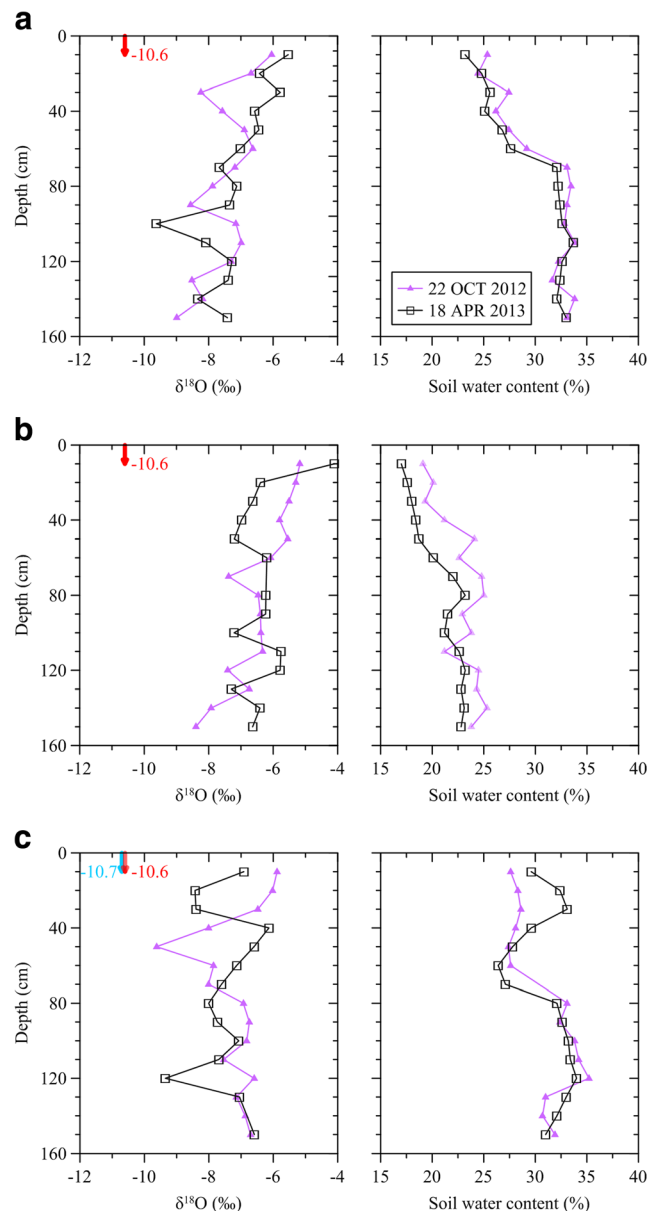


Fig. 8 Vertical profiles of soil-water $\delta^{18}\text{O}$ values and soil-water content (percent by volume) observed on 22 October 2012 and 18 April 2013 at the three sites: **a** A, **b** B and **c** C. The accuracy of the cryogenic vacuum extraction for soil-water $\delta^{18}\text{O}$ and $\delta^2\text{H}$ are 0.15 and 0.77‰, respectively. The sky blue arrow indicates the irrigation water from G2 well with the mean $\delta^{18}\text{O}$ value of -10.7‰ . The red arrows indicate the precipitation during the dry season with amount-weighted mean $\delta^{18}\text{O}$ value of -10.6‰

Robertson and Gazis (2006) found that the isotopic compositions of precipitation may vary between the beginning and end of a significant rainstorm. Indeed, Smith et al. (1979) had confirmed that highly variable isotopic compositions occurred in a single storm at a single station.

The stable isotopic compositions of shallow groundwater (mean: $\delta^{18}\text{O} -5.5\text{‰}$, $\delta^2\text{H} -44.9\text{‰}$) and deep groundwater (mean: $\delta^{18}\text{O} -10.7\text{‰}$, $\delta^2\text{H} -82.1\text{‰}$) were relatively constant and the temporal variances were much subdued compared with those of precipitation (Fig. 4). On the other hand, it can

be seen in Fig. 4 that shallow groundwater showed a significant decrease to more depleted isotopic values both for the $\delta^{18}\text{O}$ ($\sim -1.2\text{‰}$ change) and $\delta^2\text{H}$ ($\sim -8.9\text{‰}$ change) values from the beginning of the 2013 rainy season. As mentioned in Fig. 3 and related discussions, shallow groundwater is possibly mainly recharged during the rainy season; however, the amount-weighted mean $\delta^{18}\text{O}$ and $\delta^2\text{H}$ values of precipitation in the rainy season were much more enriched than those in the dry season. Therefore, one would hypothesize that the possibilities are: (1) precipitation and/or irrigation water in the dry season (with much depleted isotopic values) had reached the shallow groundwater, and/or (2) storm water with depleted isotopic values in the rainy season reached the groundwater through macropores by preferential flow. A similar phenomenon was also observed in the NCP (130 km north of the study area) by Song et al. (2011), who concluded that shallow groundwater recharge from precipitation mainly occurred in the rainy season, especially when rain-storms or successive heavy rain events happened.

The temporal variation of isotopic composition in precipitation, shallow groundwater and deep groundwater during the sampled period is expressed as the coefficient of variation (CV). The CVs for $\delta^{18}\text{O}$ and $\delta^2\text{H}$ were 35.2 and 35.0% (precipitation), 10.2 and 7.9% (shallow groundwater), and 2.1 and 1.0% (deep groundwater), respectively, which highlights the relative lack of variability in $\delta^{18}\text{O}$ and $\delta^2\text{H}$ in shallow groundwater and deep groundwater compared with that of the precipitation.

Studies have shown that the attenuation of temporal isotopic composition of shallow groundwater depends on the thickness of the unsaturated zone (Clark and Fritz 1997), and that the variation of shallow groundwater can be somewhat smaller than that of precipitation (Asano et al. 2002; DeWalle et al. 1997; Kabeya et al. 2007; Kortelainen and Karhu 2004; McGuire et al. 2002; O'Driscoll et al. 2005; Rodgers et al. 2005; Song et al. 2011). Song et al. (2009) found that the CV of shallow groundwater for $\delta^2\text{H}$ ranged from 13 to 9% in 2005 and 2006 at site HS (15 km southern to the present study area) with the shallow groundwater depth ranging from 2.5 to 4.5 m. The smaller CV results from the present study would be ascribed to the deeper groundwater depth (9.0 m); consequently, the isotopic variation of precipitation was integrated by the homogenization of the aquifer water.

Infiltration by a 92-mm storm based on soil-water content and $\delta^{18}\text{O}$ values

Comparison of soil-water content (percent by volume) and soil-water isotope profiles monitored before and after the 92-mm storm (Fig. 7) reveals important aspects of soil-water behavior in response to infiltration. The variations of soil-water content profiles (Fig. 7) were incongruous for the three sites though they were monitored at the same time, likely due

to the difference of soil texture (Fig. 2). At site A (Fig. 7a), the soil-water content on 24 July decreased with depth to a minimum (15.5%) at 60 cm depth, and then increased abruptly to 27.9% at 70 cm due to the evapotranspiration and soil stratification between 60 and 70 cm. It is shown in Fig. 2a that the sand content decreased dramatically and both the silt and clay content increased from 40 to 70 cm with clay content 14.3% at 70 cm and 6.7% at 40 cm, respectively. In addition, the soil-water content above 70 cm was much greater on 2, 4 and 13 August than before the 92-mm storm (on 24 July), while remaining at relatively constant content at 35% below the depth of 70 cm. As soil-water content can increase as a result of the water above it being forced downward, it is not necessarily caused by the downward percolation of precipitation from a single storm. The increasing soil-water content up to 70 cm depth on 2 August after the 92-mm storm will be discussed later via integration of the isotope data.

It is shown in Figs. 6b and 7b that the soil-water content increased from 21.1% on 24 July to 32.2% on 2 August in the upper 40 cm, indicating that the soil-water content responded to the infiltrated precipitation at site B. From then on, water uptake by root and evaporation accounted for the reducing of soil-water content in the upper 40 cm on 4 and 13 August. Meanwhile, variations of the soil-water content below 40 cm were almost negligible and stayed as low as 26.4% due to the relatively homogeneous soil lithology (Fig. 2b), implying that the precipitation input had not yet reached this depth, perhaps due to the root water uptake and evaporation at the upper soil layer (10–40 cm), or possibly bypass by preferential flow. The soil-water content below 40 cm increased slightly on 2 August and stayed overall steady. Song et al. (2009) carried out detailed correlation analysis of precipitation and soil-water potential at two sites (CZ and HS sites, in which CZ is 120 km northeast and HS is 15 km south to the present study area) of shallow groundwater areas in the NCP. Song et al. (2009) found that the soil water in the shallow depth (<30 cm) was strongly affected by precipitation and evapotranspiration.

The soil-water content at site C (Figs. 6c and 7c) showed smaller variations than at sites A and B before and after the 92-mm storm, maintaining the highest values of the three sites. Irrigation in the dry season and rainfall in the rainy season supplied the deficit of soil water in the arable land. The gutters in the arable land (site C) protect the crops from flooding. The soil-water content in the upper 70 cm increased on 2 August and decreased on 4 August to nearly the same values as on 24 July, indicating that the 92-mm storm had less effect at site C than at sites A and B.

Soil-water $\delta^{18}\text{O}$ profiles (Fig. 7) show that all of the soil-water $\delta^{18}\text{O}$ values were isotopically enriched compared to those of the 92-mm storm (amount-weighted mean $\delta^{18}\text{O} - 10.4\text{‰}$). In the top 10 cm, low water content and relatively enriched $\delta^{18}\text{O}$ values (site A -7.0‰ , site B -4.2‰ , and site C -6.1‰) on 24 July were observed even though there was a

rainstorm on 9 July with more depleted $\delta^{18}\text{O}$ values (amount 20.8 mm, $\delta^{18}\text{O} -10.1\text{‰}$). This discrepancy between the isotopically enriched 10-cm soil water on 24 July and depleted $\delta^{18}\text{O}$ values rainstorm on 9 July suggested the effect of evaporation in the superficial soil layer. After the 92-mm storm, the soil-water $\delta^{18}\text{O}$ values in the top 10 cm decreased to -9.1 and -8.3‰ at site A (Fig. 7a) and to -9.3 and -9.0‰ at site B (Fig. 7b) on 2 and 4 August, respectively. These soil-water $\delta^{18}\text{O}$ values were more depleted than those on 24 July, but slightly more enriched than those of the precipitation, indicating that the pre-existing soil water was well mixed with the infiltrated precipitation and showed the lowest residence time in the top 10-cm layer. Variability in both water content and $\delta^{18}\text{O}$ values is larger for the surface horizons than for deeper in the soil profile as the evaporation and downward flow began at the soil–atmosphere interface and worked progressively downward.

The soil water in the top 10 cm stayed enriched $\delta^{18}\text{O}$ values, after the 92-mm storm, on 2 and 4 August (-8.2 and -7.0‰) at site C (Fig. 7c) than those at sites A and B. The differences in soil-water $\delta^{18}\text{O}$ values might be explained by antecedent soil water, vegetation cover, and soil texture.

The mixing of infiltrating precipitation and antecedent soil water is dependent to some extent on soil textures and might have significant influence on the $\delta^{18}\text{O}$ values of the soil water (Brodersen et al. 2000; Hsieh et al. 1998). The soil-water content did not change much, indicating that the mixing in the shallow subsurface had the least impact at site C (Fig. 7c); moreover, small variations of soil-water $\delta^{18}\text{O}$ values before (24 July) and after (2, 4, and 13 August) the 92-mm storm also suggested that there were small portions of rainwater mixing with the antecedent soil water (Fig. 7c). The apparent lack of infiltration on isotopic signatures in the shallow subsurface at site C might indicate: (1) very slow diffuse flow, and (2) the likelihood that infiltration was incorporated through preferential flow. It is shown in Fig. 7c that there were some soil-water-depleted $\delta^{18}\text{O}$ spikes below 50 cm which were not seen on 24 July, before the 92-mm rainstorm, indicating that some rainwater reached below 50 cm bypassing the upper soils, and the preferential flow might be reasonable. On the other hand, more enriched soil-water $\delta^{18}\text{O}$ values on 13 August were -6.3‰ (site A), -6.7‰ (site B), and -6.6‰ (site C) at 10 cm depth (Fig. 7) could be attributed largely to evaporation and secondarily to the infiltrated precipitation with enriched isotopic composition that occurred on 12 August ($\delta^{18}\text{O} = -5.9\text{‰}$).

In the top 10–40 cm at sites A and C and 10–60 cm at site B, soil-water $\delta^{18}\text{O}$ values before the 92-mm storm (24 July) were more enriched at site B (mean value -4.6‰) than that at sites A and C (mean values -6.6 and -6.6‰ , Fig. 7). As soil water is not significantly fractionated by plant transpiration so that root uptake does not affect the isotopic composition of soil water (Dawson and Ehleringer 1991; Sharma and Hughes

1985; Turner et al. 1987), the more enriched $\delta^{18}\text{O}$ values would largely be ascribed to the much stronger evaporation fractionation effect in the poplar land (site B) than that in the grassland (site A) and arable land (site C). The three sites are within ~ 3 km of each other and the variance of amount and isotopic compositions in precipitation are insignificant. Previous studies concluded that evaporation and isotopic exchange with the atmospheric water vapor would lead in most cases to an isotopic enrichment of intercepted water (Saxena 1987), though the enrichment were only 0.17 – 0.32‰ in central Pennsylvania, USA (DeWalle and Swistock 1994) and 0.36 – 0.38‰ in the mountainous ‘Black Forest’ region of southern Germany (Brodersen et al. 2000). Therefore, one could make a hypothesis that the more enriched soil-water $\delta^{18}\text{O}$ values in the poplar land (site B) than that in the grassland (site A) and arable land (site C) was somewhat due to the different isotopic input precipitation to the soil surface.

After the 92-mm storm, soil-water $\delta^{18}\text{O}$ values at depths of 10–40 cm at sites A (mean -7.9‰) and C (mean -7.4‰) and 10–60 cm at site B (mean -6.7‰) observed on 2 August were more depleted than those on 24 July (Fig. 7), indicating that a substantial proportion of antecedent soil water was mixed with the 92-mm storm infiltration (-10.4‰). Notably, increasing soil-water content in the upper 40 cm at the three sites (Fig. 7) confirmed that some portion of precipitation might reach this depth. A detailed oxygen isotope study in precipitation and soil water by Robertson and Gazis (2006) observed that the pre-existing soil water was of great significance in controlling the ^{18}O signal in soil water, and therefore in distinguishing the proportion of infiltrated water. Assuming that the soil water on 2 August is a mixture of the 92-mm storm (mean $\delta^{18}\text{O} -10.4\text{‰}$) and antecedent soil water (collected on 24 July), isotopic mass balance considerations estimate the proportion of antecedent soil water to be 61, 17 and 78% at 10 cm, and 65, 62 and 78% at 10–40 cm depth intervals at sites A and B and C, respectively. An interesting phenomenon at the three sites when the 92-mm storm occurred, is that $\delta^{18}\text{O}$ and $\delta^2\text{H}$ values in the soil water were more depleted on 4 August than on 2 August 2012, probably because local heterogeneities cause variability in samples not taken from the same spot.

Influence of irrigation infiltration

The soil profiles on 22 October 2012 and 18 April 2013 were obtained 10 and 2 days later after irrigation at site C, respectively. The soil-water deficit was as small during the dry season (October to the following May) as during the rainy season (Figs. 7c and 8c). This highlights the influence of irrigation on soil water in the arable land during the dry season. On the other hand, the soil-water profile on 13 August (Fig. 7c) showed relatively more enriched $\delta^{18}\text{O}$ values (-7.7 – -6.6‰) from 10 to 80 cm, and the $\delta^{18}\text{O}$ values of precipitation during 18 August and 4 October ranged from -8.6 to -4.8‰ . As

evaporation effects frequently cause more enriched $\delta^{18}\text{O}$ values in the residual water (Clark and Fritz 1997), one could reasonably argue that the depleted $\delta^{18}\text{O}$ spike (Fig. 8c) with value -9.6‰ at 50 cm (22 October 2012) resulted from irrigation water (mean $\delta^{18}\text{O} -10.7\text{‰}$). Moreover, there was less precipitation in the dry season (Fig. 5) with relatively depleted $\delta^{18}\text{O}$ values (-9.8 – 7.2‰); therefore, the depleted $\delta^{18}\text{O}$ spike (-8.4‰) at 20–30 cm on 18 April 2013 might derive from typical mixing of irrigation water and winter precipitation or snowmelt. Continuous mixing of precipitation and irrigation with depleted $\delta^{18}\text{O}$ values might account for the smaller differences between the upper and lower horizon values (Figs. 7c and 8c). Consequently, the soil-water content and $\delta^{18}\text{O}$ profiles at site C are very different from those at sites A and B that had no irrigation, which also confirmed that the irrigation water played an important role in the groundwater circulation (Lin et al. 2013; Ma et al. 2016; Sun et al. 2015; Wang et al. 2008). In addition, the isotopically depleted spikes of soil-water $\delta^{18}\text{O}$ at 120 cm were nearly the same on 4 August 2012 (-9.6‰ , Fig. 7c) and 18 April 2013 (-9.4‰ , Fig. 8c), possibly by chance. Another possibility is that irrigation water (applied 2 days before the soil profile sampling, mean $\delta^{18}\text{O} -10.7\text{‰}$) reached this depth by preferential flow.

At sites A and B, the soil profiles showed relatively lower soil-water content and enriched $\delta^{18}\text{O}$ values than those in the rainy season in the upper layers (10–90 cm at site A and 10–120 cm at site B; Figs. 7a,b and 8a,b), and soil-water content increased with depth, while the soil-water $\delta^{18}\text{O}$ decreased with depth. Below those depths the soil-water content and $\delta^{18}\text{O}$ profiles showed little change for the entire season, implying that the deeper the soil profiles, the more homogenized are the isotope values due to dispersion. This trend also highlighted that the upper horizons of the unsaturated soil were impacted by water flow more than the deeper horizons—for example, in the case of site A covered by grass (Fig. 8a), the soil-water $\delta^{18}\text{O}$ decreased from -6.1 to -8.6‰ on 22 October 2012 (10–90 cm) with an abrupt depleted $\delta^{18}\text{O}$ spike at 30 cm depth ($\delta^{18}\text{O} = -8.2\text{‰}$), while on 18 April 2013, the soil-water $\delta^{18}\text{O}$ decreased gradually from -5.5 to -9.6‰ (10–100 cm) mainly due to water flow and mixing within the soil profile.

Subsurface water flow pathways

As preferential flow frequently results in isotopic composition spikes (isotopically depleted or enriched soil water) deeper in the soil profile, the soil-water depleted $\delta^{18}\text{O}$ value spikes on 4 August at 120 cm depth ($\delta^{18}\text{O} -8.1\text{‰}$) and on 13 August at 130 cm depth ($\delta^{18}\text{O} -8.4\text{‰}$) were not seen at the same depth on 24 July and 2 August at site B (Fig. 7b). This observation indicated that some isotopically depleted precipitation moved by preferential flow through the shallow soil through macropores and mixed with isotopically enriched pre-

existing soil water at 120 and 130 cm depths. It is also interesting to note that there was no depleted $\delta^{18}\text{O}$ spike in the profile on 2 August, indicating that there was some delay in transmission of isotopically depleted precipitation to the 120 cm depth (Fig. 7b). Site B has been poplar land for more than 20 years and local heterogeneities like the macropores produced by root casts would be the likely source of macropores. Meanwhile, the local heterogeneities would explain the absence of a soil-water-depleted isotopic spike on 2 August.

At site C, depleted $\delta^{18}\text{O}$ spikes at 50, 70, 130, and 150 cm depths on 2 August, at 120 cm on 4 August, and at 100 cm on 13 August, which were not seen on 24 July (Fig. 7c), also indicated preferential flow pathways. Furthermore, some depleted $\delta^{18}\text{O}$ spike depths were much deeper on 2 August (130 and 150 cm) than those on 4 August (120 cm) and 13 August (100 cm). One hypothesis is that there are two possible reasons—firstly, there was upward water movement, and this likely would cause soil-water isotopic mixing. The more-depleted $\delta^{18}\text{O}$ values (-9.6‰) on 4 August at 120 cm than that on 2 August at 130 and 150 cm (-8.8 and -9.2‰) indicated that the upward mixing process was probably not the explanation. Secondly, the depleted $\delta^{18}\text{O}$ spikes on 4 and 13 August were caused by water flowing more slowly through some different macropore systems, which had different hydraulic conductivities.

Several studies provided evidence of preferential flow bypassing upper soil layers by studying the stable isotopic compositions of precipitation and soil water (Gazis and Feng 2004; Liu et al. 2015; O'Driscoll et al. 2005; Song et al. 2009; Stumpp and Maloszewski 2010; Zhao et al. 2013). A soil column experiment conducted by Milville (1990) showed that direct preferential infiltration bypassed the soil matrix and reached the depth of 140 cm in less than a day. The field data conducted by Mathieu and Bariac (1996) also revealed that direct infiltration along macropores of non-fractionated rainwater reached the 100–200-cm depth soil layer shortly after precipitation of more than 10 mm, while the upper soil layer remaining unaffected.

The antecedent soil-water content at site B (Figs. 6b and 7b) was overall much lower than at site C (Figs. 6c and 7c). Meanwhile, it was found while sampling, that thick root penetration was highly visible down to 130 cm (site B), which additionally supports the hypothesis of the anomalies arising from preferential flow of earlier precipitation through macropores (Hardie et al. 2011; Hangen et al. 2005; Liu et al. 2015; Nimmo 2012; Nimmo and Mitchell 2013). Some studies have observed greater preferential flow at higher antecedent soil-water content (Jaynes et al. 2001; Kung et al. 2000), and some at lower antecedent soil-water content (Hardie et al. 2011; Liu et al. 2015; Zhao et al. 2013). Evidence was found for preferential flow at sites B (low soil-water content) and C (high soil-water content), though not at A.

The depleted soil-water $\delta^{18}\text{O}$ spikes in the poplar land and arable land (Fig. 7b,c) also indicated that the preferential flow was dominant when the high-intensity 92-mm rainstorm occurred. These results are consistent with studies by Stumpp and Maloszewski (2010), in which high-intensity storms contributed a larger proportion of preferential flow relative to diffuse flow, but contrast with studies such as those of Zhao et al. (2013) and Liu et al. (2015), in which high rain intensity favors diffuse flow and the small precipitation events could generate recharge by preferential flow. In this study, soil-water $\delta^{18}\text{O}$ profiles at site A (Fig. 7a), however, indicate diffuse flow. The pre-existing soil water with more enriched $\delta^{18}\text{O}$ values moved from 30 cm (24 July, $\delta^{18}\text{O} -6.0\text{‰}$) to 50 cm (2 August, $\delta^{18}\text{O} -6.6\text{‰}$) and 70 cm (13 August, $\delta^{18}\text{O} -6.2\text{‰}$), showing that the input rainwater successively displaced pre-existing mobile soil water pushing it downward. The observed depleted soil $\delta^{18}\text{O}$ values in the upper 40 cm soil layer on 2 and 4 August at site A (Fig. 7a) indicated that rainwater first fills up soil pores in the 10–40-cm soil layer by diffuse flow, consistent with results reported by Dahlke et al. (2012), Gazis and Feng (2004), and Zhao et al. (2013). This suggested that antecedent soil-water content and rain intensity did not always play a crucial role in preferential flow, and that vegetation type and soil texture were also very important to flow pathways in the unsaturated zone. It can be seen in Fig. 2 that the proportion of sand in the top 40 cm is as high as 27.9–39.4% in the grassland (site A), which indicates that the sandier the soils, the less likely overland flow will occur and the greater the chances of diffuse flow.

Conclusions

Stable isotopes ($\delta^{18}\text{O}$ and $\delta^2\text{H}$) in precipitation were investigated on a daily basis, and in shallow groundwater (<50 m) and deep groundwater (230 m) on a biweekly basis, from Apr. 2012 to Oct. 2013 in the central alluvial and lacustrine plain of NCP, to give insight into the temporal variations and transition between the precipitation and groundwater. Soil-water stable isotopes down to 150 cm, at 10-cm intervals, covered by grass (*C. humili* and *C. lanceolata*; site A), poplar (*P. hopeiensis*; site B) and winter wheat (*T. aestivum*) and summer maize (*Z. mays*; site C) in different seasons from 2012 to 2013, were extracted to understand the subsurface water flow pathways. The following conclusions can be drawn.

Firstly, the $\delta^{18}\text{O}$ and $\delta^2\text{H}$ values in shallow groundwater (deep < 50 m) were relatively constant compared to that of the precipitation for the whole year, which suggested the complete mixing of different input waters during the recharge period to the shallow groundwater in this area. The deep groundwater (deep 230 m) used for irrigation is more depleted in $\delta^{18}\text{O}$ and $\delta^2\text{H}$ than the local precipitation and shallow groundwater,

reflecting a meteoric origin during a period of colder climate with isotopically lighter composition, or lateral flow from the surrounding mountain areas.

Secondly, the soil-water data collected at three vegetated sites indicated that the $\delta^{18}\text{O}$ values of soil water in the shallowest 10 cm depth was significantly affected by both evaporation and infiltration. Water in the shallow 10–40-cm interval depth showed a relatively short residence time as a substantial antecedent soil water was mixed with the 92-mm storm infiltration. The antecedent soil-water fractions decreased and showed longer residence time with increasing depth. These data also indicated that diffuse flow and preferential flow coexisted for the various vegetated soils at a small scale. The local heterogeneities affected the subsurface water flow pathways. Preferential flow was common within the active plant root zone both in the poplar and arable land. The grassland with high soil-water content produced diffuse flow, which highlighted that the unsaturated water flow pathways were affected by comprehensive factors including antecedent soil moisture content, vegetation type, precipitation intensity, and soil texture.

Acknowledgements This research was funded by the National Basic Research Program of China (2010CB428802) and the National Natural Science Foundation of China (U1403282). The authors would like to thank Randy Bayless, Christine Stumpp, Dongmei Han, and Hongbing Zhan for their valuable discussions and suggestions for this paper. We wish to thank Dan Lin, Siyuan Huo, Changkun Zhu, Yalei Liu and Lan Yang for sampling and laboratory works. We also wish to thank the editor and reviewers for their useful comments and encouragement.

References

- Allen ST, Keim RF, McDonnell JJ (2015) Spatial patterns of throughfall isotopic composition at the event and seasonal timescales. *J Hydrol* 522:58–66. doi:10.1016/j.jhydrol.2014.12.029
- Allison GB, Barnes CJ (1983) Estimation of evaporation from non-vegetated surfaces using natural deuterium. *Nature* 301:143–145. doi:10.1038/301143a0
- Araguás-Araguás L, Rozanski K, Gonfiantini R, Louvat D (1995) Isotope effects accompanying vacuum extraction of soil water for stable isotope analyses. *J Hydrol* 168:159–171
- Asano Y, Uchida T, Ohte N (2002) Residence times and flow paths of water in steep unchannelled catchments, Tanakami, Japan. *J Hydrol* 261:173–192
- Barnes CJ, Allison GB (1988) Tracing of water movement in the unsaturated zone using stable isotopes of hydrogen and oxygen. *J Hydrol* 100:143–176
- Broderson C, Pohl S, Lindenlaub M, Leibundgut C, Wilpert KV (2000) Influence of vegetation structure on isotope content of throughfall and soil water. *Hydrol Process* 14:1439–1448
- Chen ZY, Qi JX, Xu JM, Xu JM, Ye H, Nan YJ (2003) Paleoclimatic interpretation of the past 30 ka from isotopic studies of the deep confined aquifer of the North China plain. *Appl Geochem* 18:997–1009
- Clark ID, Fritz P (1997) *Environmental isotopes in hydrogeology*. CRC, Boca Raton, FL, 328 pp

- Craig H (1961) Isotopic variations in meteoric waters. *Science* 133:1702–1703
- Dahlke HE, Easton ZM, Lyon SW, Walter MT, Destouni G, Steenhuis TS (2012) Dissecting the variable source area concept: subsurface flow pathways and water mixing processes in a hillslope. *J Hydrol* 420–421:125–141. doi:10.1016/j.jhydrol.2011.11.052
- Darling WG, Bath AH (1988) A stable isotope study of recharge processes in the English Chalk. *J Hydrol* 101:31–46
- Dawson TE, Ehleringer JR (1991) Streamside trees that do not use stream water. *Nature* 350:335–337
- DeWalle DR, Swistock BR (1994) Differences in oxygen-18 content of throughfall and rainfall in hardwood and coniferous forests. *Hydrol Process* 8:75–82
- DeWalle DR, Edwards PJ, Swistock BR, Aravena R, Drimmie RJ (1997) Seasonal isotope hydrology of three Appalachian forest catchments. *Hydrol Process* 11:1895–1906
- Foster S, Garduno H, Evans R, Olson D, Tian Y, Zhang W, Han Z (2004) Quaternary aquifer of the North China Plain: assessing and achieving groundwater resource sustainability. *Hydrogeol J* 12:81–93. doi:10.1007/s10040-003-0300-6
- Gaziz C, Feng XH (2004) A stable isotope study of soil water: evidence for mixing and preferential flow paths. *Geoderma* 119:97–111. doi:10.1016/S0016-7061(03)00243-X
- Gee GW, Or D (2002) 2.4 Particle-size analysis. *Methods of soil analysis: part 4, physical methods, (methods of soil analysis 4)*. SSSA, Washington, DC, pp 255–293
- Gonfiatini R (1978) Standards of stable isotope measurement in natural compounds. *Nature* 271:534–536. doi:10.1038/271534a0
- Gong B, Zheng YF, Chen RX (2007) TC/EA-MS online determination of hydrogen isotope composition and water concentration in eclogitic garnet. *Phys Chem Minerals* 34:687–698. doi:10.1007/s00269-007-0184-4
- Hangen E, Gerke HH, Schaaf W, Hüttl RF (2005) Assessment of preferential flow processes in a forest-reclaimed lignitic mine soil by multicell sampling of drainage water and three tracers. *J Hydrol* 303:16–37. doi:10.1016/j.jhydrol.2004.07.009
- Hardie MA, Cotching WE, Doyle RB, Holz G, Lisson S, Mattern K (2011) Effect of antecedent soil moisture on preferential flow in a texture-contrast soil. *J Hydrol* 398:191–201. doi:10.1016/j.jhydrol.2010.12.008
- Hopp L, McDonnell JJ (2009) Connectivity at the hillslope scale: identifying interactions between storm size, bedrock permeability, slope angle and soil depth. *J Hydrol* 376:378–391. doi:10.1016/j.jhydrol.2009.07.047
- Hsieh JCC, Chadwick OA, Kelly EF, Savin SM (1998) Oxygen isotopic composition of soil water: quantifying evaporation and transpiration. *Geoderma* 82:269–293
- Huo SY, Jin MG, Liang X, Lin D (2014) Changes of vertical groundwater recharge with increase in thickness of vadose zone simulated by one-dimensional variably saturated flow model. *J Earth Sci* 25(6):1043–1050. doi:10.1007/s12583-014-0486-7
- Ignatev A, Velivetchkaia T, Sugimoto A, Ueta A (2013) A soil water distillation technique using He-purging for stable isotope analysis. *J Hydrol* 498:265–273. doi:10.1016/j.jhydrol.2013.06.032
- Ingraham NL, Shadel C (1992) A comparison of the toluene distillation and vacuum/heat methods for extracting soil water for stable isotopic analysis. *J Hydrol* 140:371–387
- Jaynes DB, Ahmed SI, Kung KJS, Kanwar RS (2001) Temporal dynamics of preferential flow to a subsurface drain. *Soil Sci Soc Am J* 65:1368–1376
- Jin MG, Zhang RQ, Sun LF, Gao YF (1999) Temporal and spatial soil water management: a case study in Heilonggang region, PR China. *Agric Water Manag* 42:173–187
- Jin MG, Liang X, Simmers I, Gao YF, Zhang RQ (2000) Estimation of groundwater recharge using artificial tritium tracing. In: *Proceedings of the International Symposium on Hydrogeology and the Environment*, Wuhan, China, 17–21 October 2000. China Environmental Science Press, Beijing, pp 340–345
- Kabeya N, Katsuyama M, Kawasaki M, Ohte N, Sugimoto A (2007) Estimation of mean residence times of subsurface waters using seasonal variation in deuterium excess in a small head water catchment in Japan. *Hydrol Process* 21:308–322. doi:10.1002/hyp.6231
- Koeniger P, Marshall JD, Link T, Mulch A (2011) An inexpensive, fast, and reliable method for vacuum extraction of soil and plant water for stable isotope analyses by mass spectrometry. *Rapid Commun Mass Spectrom* 25:3041–3048. doi:10.1002/rcm.5198
- Kortelainen NM, Karhu JA (2004) Regional and seasonal trends in the oxygen and hydrogen isotope ratios of Finnish groundwaters: a key for mean annual precipitation. *J Hydrol* 285:143–157. doi:10.1016/j.jhydrol.2003.08.014
- Kung KJS, Steenhuis TS, Kladvik EJ, Gish TJ, Bubenzer G, Helling CS (2000) Impact of preferential flow on the transport of adsorbing and non-adsorbing tracers. *Soil Sci Soc Am J* 64:1290–1296
- Landon MK, Delin GN, Komor SC, Regan CP (1999) Comparison of the stable-isotopic composition of soil water collected from suction lysimeters, wick samplers, and cores in a sandy unsaturated zone. *J Hydrol* 224:45–54
- Lee KS, Kim JM, Lee DR, Kim Y, Lee D (2007) Analysis of water movement through an unsaturated soil zone in Jeju Island, Korea using stable oxygen and hydrogen isotopes. *J Hydrol* 345:199–211. doi:10.1016/j.jhydrol.2007.08.006
- Li FD, Song XF, Tang CY, Liu CM, Yu JJ, Zhang WJ (2007) Tracing infiltration and recharge using stable isotope in Taihang Mt., North China. *Environ Geol* 53:687–696. doi:10.1007/s00254-007-0683-0
- Li XZ, Shao MA, Jia XX, Wei XR, He L (2015) Depth persistence of spatial pattern of soil-water storage along a small transect in the Loess Plateau of China. *J Hydrol* 529:685–695. doi:10.1016/j.jhydrol.2015.08.039
- Lin D, Jin MG, Liang X, Zhan HB (2013) Estimating groundwater recharge beneath irrigated farmland using environmental tracers fluoride, chloride and sulfate. *Hydrogeol J* 21:1469–1480. doi:10.1007/s10040-013-1015-y
- Liu BL, Phillips F, Hoines S, Campbell AR, Sharma P (1995) Water movement in desert soil traced by hydrogen and oxygen isotopes, chloride, and chlorine-36, southern Arizona. *J Hydrol* 168:91–110
- Liu JR, Song XF, Yuan GF, Sun XM, Liu X, Wang SQ (2010) Characteristics of $\delta^{18}\text{O}$ in precipitation over Eastern Monsoon China and the water vapor sources. *Chinese Sci Bull* 55:200–211. doi:10.1007/s11434-009-0202-7
- Liu YH, Liu FD, Xu Z, Zhang JP, Wang LX, An SQ (2015) Variations of soil water isotopes and effective contribution times of precipitation and throughfall to alpine soil water, in Wolong Nature Reserve, China. *Catena* 126:201–208. doi:10.1016/j.catena.2014.11.008
- Lv MX, Hao ZC, Liu Z, Yu ZB (2013) Conditions for lateral downslope unsaturated flow and effects of slope angle on soil moisture movement. *J Hydrol* 486:321–333. doi:10.1016/j.jhydrol.2013.02.013
- Ma FJ, Gao H, Eneji AE, Jin ZZ, Han LP, Liu JT (2016) An economic valuation of groundwater management for agriculture in Luancheng county, North China. *Agric Water Manag* 163:28–36. doi:10.1016/j.agwat.2015.08.027
- Mathieu R, Bariac T (1996) An isotopic study (^2H and ^{18}O) of water movements in clayey soils under a semiarid climate. *Water Resour Res* 32(4):779–789
- McGuire KJ, DeWalle DR, Gburek WJ (2002) Evaluation of mean residence time in subsurface waters using oxygen-18 fluctuations during drought conditions in the mid-Appalachians. *J Hydrol* 261:132–149
- Milville F (1990) Contribution à l'étude des mécanismes de la recharge naturelle des aquifères par les pluies en climat semi-aride: application au site expérimental de Barogo au Burkina Faso [Contribution to the study of the mechanisms of natural recharge of aquifers by rainfall in a semi-arid climate: application to the experimental site of

- Barogo in Burkina Faso]. PhD Thesis, Univ. Pierre et Marie Curie, Paris, 216 pp
- Mueller MH, Alauui A, Kuells C, Leister H, Meusbürger K, Stumpp C, Weiler M, Alewell C (2014) Tracing water pathways in steep hillslopes by $\delta^{18}\text{O}$ depth profiles of soil water. *J Hydrol* 519:340–352. doi:10.1016/j.jhydrol.2014.07.031
- Nimmo JR (2005) Unsaturated zone flow processes. In: Anderson MG, Bear J (eds) *Encyclopedia of hydrological sciences: part 13, groundwater*, vol 4. Wiley, Chichester, UK, pp 2299–2322. doi:10.1002/0470848944.hsa161
- Nimmo JR (2010) Theory for source-responsive and free-surface film modeling of unsaturated flow. *Vadose Zone J* 9:295–306. doi:10.2136/vzj2009.0085
- Nimmo JR (2012) Preferential flow occurs in unsaturated conditions. *Hydrol Process* 26:786–789. doi:10.1002/hyp.8380
- Nimmo JR, Mitchell L (2013) Predicting vertically nonsequential wetting patterns with a source-responsive model. *Vadose Zone J*. doi:10.2136/vzj2013.03.0054
- O'Driscoll MA, DeWalle DR, McGuire KJ, Gburek WJ (2005) Seasonal ^{18}O variations and groundwater recharge for three landscape types in central Pennsylvania, USA. *J Hydrol* 303:108–124. doi:10.1016/j.jhydrol.2004.08.020
- Orlowski N, Frede HG, Brüggemann N, Breuer L (2013) Validation and application of a cryogenic vacuum extraction system for soil and plant water extraction for isotope analysis. *J Sens Sens Syst* 2:179–193. doi:10.5194/jsss-2-179-2013
- Orlowski N, Breuer L, McDonnell JJ (2016) Critical issues with cryogenic extraction of soil water for stable isotope analysis. *Ecohydrol* 9:3–10. doi:10.1002/eco.1722
- Revesz K, Woods PH (1990) A method to extract soil water for stable isotope analysis. *J Hydrol* 115:397–406
- Robertson JA, Gazis CA (2006) An oxygen isotope study of seasonal trends in soil water fluxes at two sites along a climate gradient in Washington state (USA). *J Hydrol* 328:375–387. doi:10.1016/j.jhydrol.2005.12.031
- Rodgers P, Soulsby C, Waldron S (2005) Stable isotope tracers as diagnostic tools in upscaling flow path understanding and residence time estimates in a mountainous mesoscale catchment. *Hydrol Process* 19:2291–2307. doi:10.1002/hyp.5677
- Rohden C, Kreuzer A, Chen ZY, Kipfer R, Hertig WA (2010) Characterizing the recharge regime of the strongly exploited aquifers of the North China Plain by environmental tracers. *Water Resour Res* 46, W05511. doi:10.1029/2008WR007660
- Rusjan S, Brilly M, Mikoš M (2008) Flushing of nitrate from a forested watershed: an insight into hydrological nitrate mobilization mechanisms through seasonal high-frequency stream nitrate dynamics. *J Hydrol* 354:187–202. doi:10.1016/j.jhydrol.2008.03.009
- Saxena RK (1987) Oxygen- ^{18}O fractionation in nature and estimation of groundwater recharge. Report series A, no. 40, PhD Thesis, Uppsala University, 152 pp
- Sharma ML, Hughes MW (1985) Groundwater recharge estimation using chloride, deuterium and oxygen-18 profiles in the deep coastal sands of Western Australia. *J Hydrol* 81:93–109
- Shi JS, Li GM, Liang X, Chen ZY, Shao JL, Song XF (2014) Evolution mechanism and control of groundwater in the North China Plain (in Chinese with English abstract). *Acta Geosci Sin* 35(5):527–534. doi:10.3975/cagsb.2014.05.01
- Shurbaji AM, Phillips FM (1995) Application of a numerical model for simulating water flow, isotope transport, and heat transfer in the unsaturated zone. *J Hydrol* 171:143–163
- Smith GI, Friedman I, Klieforth H, Hardcastle K (1979) Areal distribution of deuterium in eastern California precipitation, 1968–1969. *J Appl Meteorol* 18:172–188
- Song XF, Wang SQ, Xiao GQ, Wang ZM, Liu X, Wang P (2009) A study of soil water movement combining soil water potential with stable isotopes at two sites of shallow groundwater areas in the North China Plain. *Hydrol Process* 23:1376–1388. doi:10.1002/hyp.7267
- Song XF, Wang P, Yu JJ, Liu X, Liu JR, Yuan RQ (2011) Relationships between precipitation, soil water and groundwater at Chongling catchment with the typical vegetation cover in the Taihang mountainous region, China. *Environ Earth Sci* 62:787–796. doi:10.1007/s12665-010-0566-7
- Stumpp C, Hendry MJ (2012) Spatial and temporal dynamics of water flow and solute transport in a heterogeneous glacial till: the application of high-resolution profiles of $\delta^{18}\text{O}$ and $\delta^2\text{H}$ in pore waters. *J Hydrol* 438–439:203–214. doi:10.1016/j.jhydrol.2012.03.024
- Stumpp C, Maloszewski P (2010) Quantification of preferential flow and flow heterogeneities in an unsaturated soil planted with different crops using the environmental isotopes $\delta^{18}\text{O}$. *J Hydrol* 394:407–415. doi:10.1016/j.jhydrol.2010.09.014
- Stumpp C, Maloszewski P, Stichler W, Fank J (2009a) Environmental isotope ($\delta^{18}\text{O}$) and hydrological data to assess water flow in unsaturated soils planted with different crops: case study lysimeter station “Wagna” (Austria). *J Hydrol* 369:198–208. doi:10.1016/j.jhydrol.2009.02.047
- Stumpp C, Stichler W, Maloszewski P (2009b) Application of the environmental isotope $\delta^{18}\text{O}$ to study water flow in unsaturated soils planted with different crops: case study of a weighable lysimeter from the research field in Neuheberg, Germany. *J Hydrol* 368:68–78. doi:10.1016/j.jhydrol.2009.01.027
- Sugimoto A, Naito D, Yanagisawa N, Ichianagi K, Kurita N, Kubota J, Kotake T, Ohata T, Maximov TC, Fedorov AN (2003) Characteristics of soil moisture in permafrost observed in East Siberian taiga with stable isotopes of water. *Hydrol Process* 17:1073–1092. doi:10.1002/hyp.1180
- Sun HY, Zhang XY, Wang EL, Chen SY, Shao LW (2015) Quantifying the impact of irrigation on groundwater reserve and crop production: a case study in the North China Plain. *European J Agron* 70:48–56. doi:10.1016/j.eja.2015.07.001
- Turner JV, Arad A, Johnston CD (1987) Environmental isotope hydrology of salinized experimental catchments. *J Hydrol* 94:89–107
- Walker GR, Woods PH, Allison GB (1994) Interlaboratory comparison of methods to determine the stable isotope composition of soil water. *Chem Geol (Isotope Geoscience Section)* 111:297–306
- Wang BG, Jin MG, Nimmo JR, Yang L, Wang WF (2008) Estimating groundwater recharge in Hebei Plain, China under varying land use practices using tritium and bromide tracers. *J Hydrol* 356:209–222. doi:10.1016/j.jhydrol.2008.04.011
- Wang WZ, Yoshimura K, Okazaki A, Ono K, Kim W, Yokoi M, Lai CT (2016) Understanding the variability of water isotopologues in near-surface atmospheric moisture over a humid subtropical rice paddy in Tsukuba, Japan. *J Hydrol* 533:91–102. doi:10.1016/j.jhydrol.2015.11.044
- West AG, Patrickson SJ, Ehleringer JR (2006) Water extraction times for plant and soil materials used in stable isotope analysis. *Rapid Commun Mass Spectrom* 20:1317–1321. doi:10.1002/rcm.2456
- Yang P, Shibasaki R, Wu WB, Zhou QB, Chen ZX, Zha Y, Shi Y, Tang HJ (2007) Evaluation of MODIS land cover and LAI products in cropland of North China Plain using in situ measurements and Landsat TM images. *IEEE Trans Geosci Remote Sens* 45(10):3087–3097. doi:10.1109/TGRS.2007.902426
- Zhang ZH (2005) Groundwater in the vast North China Plain (in Chinese). *Chinese J Nature* 27(6):311–315
- Zhang ZH, Shi DH, Shen ZL, Zhong ZY, Xue YQ (1997) Evolution and development of groundwater environment in North China Plain under human activities (in Chinese with English abstract). *Acta Geosci Sin* 18(4):337–344
- Zhao P, Tang XY, Zhao P, Wang C, Tang JL (2013) Identifying the water source for subsurface flow with deuterium and oxygen-18 isotopes of soil water collected from tension lysimeters and cores. *J Hydrol* 503:1–10. doi:10.1016/j.jhydrol.2013.08.0